

Impact of horizontal resolution on climate model forecasts of tropical precipitation and diabatic heating for the TWP-ICE period

James Boyle¹ and Stephen A. Klein¹

Received 31 March 2010; revised 16 August 2010; accepted 23 September 2010; published 4 December 2010.

[1] In order to study the impact of horizontal resolution on climate model simulations of tropical moist processes, short-term forecasts using the Community Atmospheric Model (version 4) at several resolutions are performed for a time period encompassing the Tropical Warm Pool-International Cloud Experiment (TWP-ICE). TWP-ICE occurred in the environment of Darwin, Australia in January and February 2006. The experimental period encompasses a number of atmospheric phenomena, such as an MJO passage, mesoscale convective systems, monsoon trough, and active and dry conditions. The CAM is run with four horizontal resolutions: 2° , 1° , 0.5° , and 0.25° latitude-longitude. Simulated profiles of diabatic heating and moistening at the TWP-ICE site show that the model parameterizations respond reasonably well for all resolutions to the sequence of varying conditions imposed by the analyses used to initialize the model. The spatial patterns of global model biases in time mean precipitation are largely unchanged over resolutions, and in some regions the 0.25° model significantly overestimates the observed precipitation. However, there are substantive positive aspects of finer resolution. The diurnally forced circulations over the Maritime continent are more realistically captured by the 0.25° simulation, which is able to better resolve the land-sea breeze. The intensity distribution of rainfall events is also improved at higher resolution through an increased frequency of very intense events and an increased frequency of little or no precipitation. Finally, the ratio of stratiform to convective precipitation systematically increases toward better agreement with observational estimates with increases in resolution.

Citation: Boyle, J., and S. A. Klein (2010), Impact of horizontal resolution on climate model forecasts of tropical precipitation and diabatic heating for the TWP-ICE period, *J. Geophys. Res.*, 115, D23113, doi:10.1029/2010JD014262.

1. Introduction

[2] This paper assesses the impact of increasing the horizontal resolution of a global climate model on the simulation of tropical moist processes. The horizontal resolution of the model is varied over a factor of eight (0.25° to 2°). The method used is to run the climate model, the Community Atmospheric Model (CAM) version 4, in forecast mode and evaluate the short-term (24–48 h) forecasts against observations. The time period chosen for the forecasts was January and February of 2006 which encompasses the Tropical Warm Pool International Cloud Experiment (TWP-ICE) experiment that was conducted in northern Australia during the monsoon season. The motivation behind the design and execution of TWP-ICE was to better understand the factors that control tropical convection. A comprehensive overview of meteorological and observational aspects of TWP-ICE is provided by May *et al.* [2008].

The observations were organized to provide a comprehensive characterization of the processes occurring on the scale of a typical general circulation model (GCM) grid cell. Figure 1 provides the geography of the experiment. The strategy is to use the observations in the TWP-ICE region to document model performance and as a reference point when examining model performance over the wider Tropics.

[3] There is a long and rich history of experiments addressing the effects of changing the horizontal resolution of GCMs, from which we note the following results that pertain to the simulation of tropical moist processes. Neale and Slingo [2003] carried out experiments to investigate the effects of horizontal resolution on tropical rainfall with emphasis on the Maritime Continent (MC). Seventeen year integrations were carried out using the United Kingdom Meteorological Office HadAM3 GCM at horizontal spacing of $2.5^\circ \times 3.75^\circ$, $1.67^\circ \times 2.5^\circ$, $1.25^\circ \times 1.875^\circ$ and $0.83^\circ \times 1.25^\circ$ with prescribed monthly mean SSTs. Their results indicate that the diurnal cycle over the islands and the complex circulation patterns generated by land-sea contrasts are crucial for the energy and hydrological cycles of the Maritime Continent and for determining the mean climate of the region. They conclude that at least part of the HadAM3's

¹Lawrence Livermore National Laboratory, Livermore, California, USA.

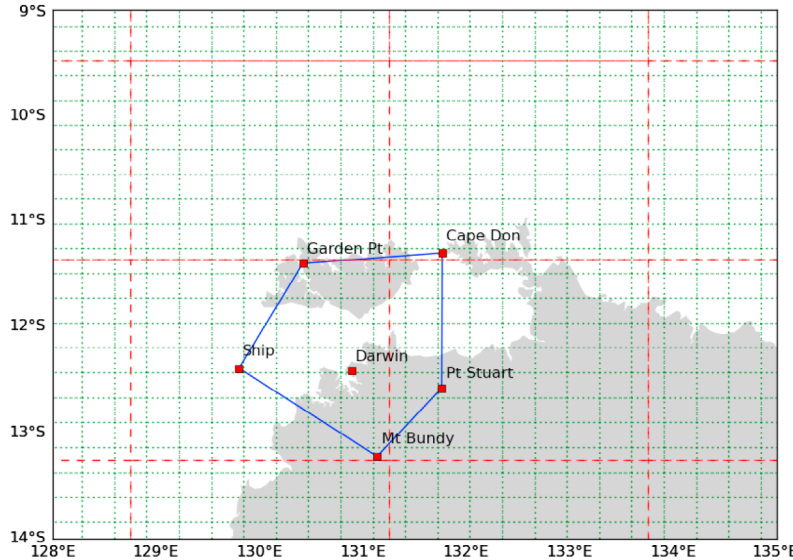


Figure 1. Locator map for key sites of the Tropical Warm Pool-International Cloud Experiment (TWP-ICE). The rawwindsonde and surface data were collected at the stations on the vertices of the polygon. Darwin was the site of the precipitation and cloud radar as well as a rawwindsonde and surface station. The radar precipitation estimates are for the region encompassed by the polygon. The dotted green lines are the boundaries of the 0.25° model grid, and the dashed red lines are the boundaries of the 2° model grid.

underestimate of the MC rainfall may be attributable to a poor simulation of the diurnal cycle and the generation of land-sea breezes around the complex system of islands of the region. Common model deficiencies persisted through all the resolutions. Hack *et al.* [2006] performed CAM 3 simulations at T85 ($\approx 1.4^\circ$) and T42 ($\approx 2.8^\circ$). They found a definite improvement in the model performance at the higher resolution. The greatest impact occurred on the larger-scale dynamical circulation. Since the resolved circulation was so much more realistic, it was felt that T85 would be a more suitable vehicle for testing parameterizations. Although the pointwise scale motions were more energetic, the energy of some large-scale modes such as the MJO did not reflect a proportional increase to more realistic values. Lau and Ploschay [2009] ran simulations of the Geophysical Fluid Dynamics Laboratory (GFDL) AM2 through the same spectrum of resolutions, 2° , 1° , 0.5° , and 0.25° , used in this work. Their focus was on the 0.5° results for the East Asian summer monsoon. The 0.5° resolution was shown to accurately depict the East Asian frontal systems and the synoptic disturbances that propagate along the front. However, the improved simulation of the mesoscale systems did not lead to a concomitant increase in the accuracy of the precipitation associated with the systems. It was noted that the higher-resolution models captured the precipitation modulation produced by topographical forcing, such as the Western Ghats but there were also instances where the higher-resolution exacerbated errors in precipitation evident on the coarser grid. Shaffrey *et al.* [2009] compared coupled simulations of the HiGEM ($0.83^\circ \times 1.25^\circ$) and HadGem ($1.25^\circ \times 1.875^\circ$) models developed at the UK Met Office. It was found that the increased resolution provided a better simulation in almost all aspects. The ocean and atmosphere-ocean interactions benefited the most from the finer grid.

They do comment on the refractory nature of the tropical precipitation errors, which are ameliorated by only a small amount in the HiGEM run.

[4] Recently, Gent *et al.* [2009] presented results of decadal coupled simulations at 2° and 0.5° resolutions using a version of CAM quite close to the one in this work. As seen in the work of Shaffrey *et al.* [2009], some of the largest impacts are found in the ocean simulation. Gent *et al.* [2009] report that the SST bias in coastal upwelling regions is reduced by 60%. The precipitation patterns in the Asian monsoon and North America are improved by going from 2° to 0.5° resolution. The authors indicate that a fair portion of the improvement is due to better resolved topography, a similar result to Lau and Ploschay [2009]. Zhao *et al.* [2009] demonstrate that a 0.5° resolution calculation using the GFDL model with modified physics parameterizations is capable of simulating the mean climatology and interannual variability of tropical cyclones of which the 2° version was not capable.

[5] A common result in these resolution studies is that the gains in going to higher resolution were fairly moderate. This is not surprising since convection remains unresolved in the finest resolution ($\approx 0.25^\circ$) used. However, many other important processes such as large-scale condensation, land-sea interaction, and topographical forcing will benefit from the resolved detail. In addition, the finer resolution has the capability to provide more representative dynamical forcing for the moist processes parameterizations. However imperfect, parameterizations can generally benefit from improved forcing.

[6] This paper brings three new elements to the large body of research on the effects of horizontal grid resolution in a global climate model. First, the climate model is used as a forecast model during a specific observational experiment.

This permits verification on the weather regimes for a specific time period and less reliance on statistical properties. The availability of special observations and analysis during the forecast period allows for the evaluation of the fast physical processes at certain locations with a level of detail often not used in GCM studies. Second, the spectrum of grid model resolutions is wide, 2° to 0.25° , and only one other study [Lau and Poshay, 2009] encompasses this breadth. This spread of resolutions encompasses the range of what is practical for global coupled model research for the immediate future. Finally, a set of integrations were performed with all the resolutions having the exact same settings of some of the poorly constrained aspects of the parameterizations. Models are usually “tuned” with arbitrary parameter settings varied to achieve in some sense (usually top of atmosphere energy balance) an optimal simulation. Here both tuned and untuned versions of the model are used, permitting a comparison whereby the *only* difference is horizontal grid resolution. This is not to say that tuning the model is in any way suspect; rather running identical versions of the model across resolutions provides a useful perspective when comparing the results.

[7] Section 1.1 will describe the observations and weather regimes of the TWP-ICE. This is followed by a description of the models used and the forecast initialization techniques. Next will be presentation of the results, followed by a discussion and conclusions.

1.1. Observations

[8] The TWP-ICE experiment combined aspects of previous observational campaigns, specifically the combination of a dense rawinsonde network and ground based radar and lidar. A part of the observational infrastructure was provided by the Department of Energy (DOE) Atmospheric Radiation Measurement (ARM) Program Climate and Research Facility (ACRF) site [Ackerman and Stokes, 2003] and another part included the Australian Bureau of Meteorology instrumentation associated with meteorological research and operational forecasting applications. May *et al.* [2008] list in detail all the instrumentation that was available during the experiment. The basic state variables of wind, temperature, and moisture were measured by rawindsondes launched every 3 h at the stations at the vertices of the polygon drawn in Figure 1. A scanning C band polarimetric radar (C-POL) located 20 km northeast of Darwin with a range of 150 km provided rainfall estimates within the polygon and tracked the evolution of convective systems. The rawindsonde data was combined with the domain averaged radar precipitation, surface energy fluxes, and top-of-the-atmosphere and surface radiative fluxes to produce an analysis of the large-scale dynamical forcing using a variational technique which constrains the sounding data to satisfy column-integrated budgets of mass, energy, and moisture [Zhang and Lin, 1997; Zhang *et al.*, 2001; Xie *et al.*, 2010a]. This variational analysis (VA) provides estimates of the profiles of apparent heating (Q_1) and drying (Q_2) [Yanai *et al.*, 1973].

[9] An ensemble VA data set has been derived for the TWP-ICE field campaign which attempts to account for the uncertainties in the radar-derived rainfall estimates. Christian Jakob (Monash University) and collaborators have estimated the possible errors in the radar-derived rainfall from a

comparison with rain gauge data and used these estimates to calculate 100 possible rainfall scenarios. Each rainfall scenario is used in the variational analysis described previously to produce an ensemble member. Each rainfall scenario is a percentile of a distribution that encompasses the full range of the errors in deriving the radar-derived rainfall and each scenario is consistent with the uncertainties in the radar-derived rainfall. The median of this ensemble is quite close to the best estimate VA analysis. These ensemble data will be used as a partial indication of the uncertainty of the observationally based heating and drying estimates.

[10] Cloud occurrence profiles were derived from the Millimeter Wavelength (35 GHz) Cloud Radar (MMCR), micropulse lidar (MPL), and laser ceilometers using the Active Remotely Sensed Clouds Locations (ARSCL) algorithm of Clothiaux *et al.* [2000]. This is a point observation from the instrument at Darwin. The instrument observation is nearly continuous and the percent indicated is the percent cloud occurrence over 3 h intervals. The ARSCL observations were obtained from the ARM Climate Model Best Estimate archive [Xie *et al.*, 2010b].

[11] For rainfall observations over the entire Tropics, the Tropical Rainfall Measuring Mission 3B42 (TRMM) data are used [Huffman *et al.*, 2007]. These are gridded data supplied every 3 h at a grid resolution of 0.25° from 50°N to 50°S and represent TRMM observations merged with other satellite estimates. To provide a measure of observational uncertainty and global coverage, the Global Precipitation Climatology Project (GPCP) rainfall observations were also used [Adler *et al.*, 2003]. These data are daily means on a 2.5° grid and are a blend of satellite estimates and rain gauge observations.

1.2. Weather During TWP-ICE

[12] Figure 2 presents the ARSCL cloud frequency and two C-POL radar precipitation estimates. The radar rainfall estimates are courtesy of Drs. Courtney Schumacher (Texas A & M University) and Timothy Hume (CSIRO). The Hume data are the values used as input to the variational analysis. The Schumacher rainfall is part of the data used for estimating vertical latent heating profiles from the C-POL radar. Both rainfall estimates are averages over the TWP-ICE polygon, Figure 1 and are provided for 1 h intervals. These time series provide a backdrop to the synoptic conditions prevalent for the TWP-ICE period. Based on May *et al.* [2008], this paper will divide the experiment period (20 January to 24 February) into three, each determined by the prevailing weather regime, (Table 1). The initial sequence of meteorological conditions was strongly influenced by the active phase of a MJO event which passed through the experiment region. The period began on 19 January with an active (Wet) monsoon characterized by westerly flow at Darwin and significant precipitation. The cloud cover was extensive with almost constant high level cloud and frequent deep convection. From 19 to 25 January a low formed in the Solomon Sea (9°S , 155°E) and moved west triggering a mesoscale convective system (MCS) that passed through Darwin. This is the very large precipitation event around 24 January, seen in Figure 2. From 26 January to 2 February, the monsoon trough moved inland and deepened substantially. This initiated the Dry period (at least in the region of Darwin). The movement of the

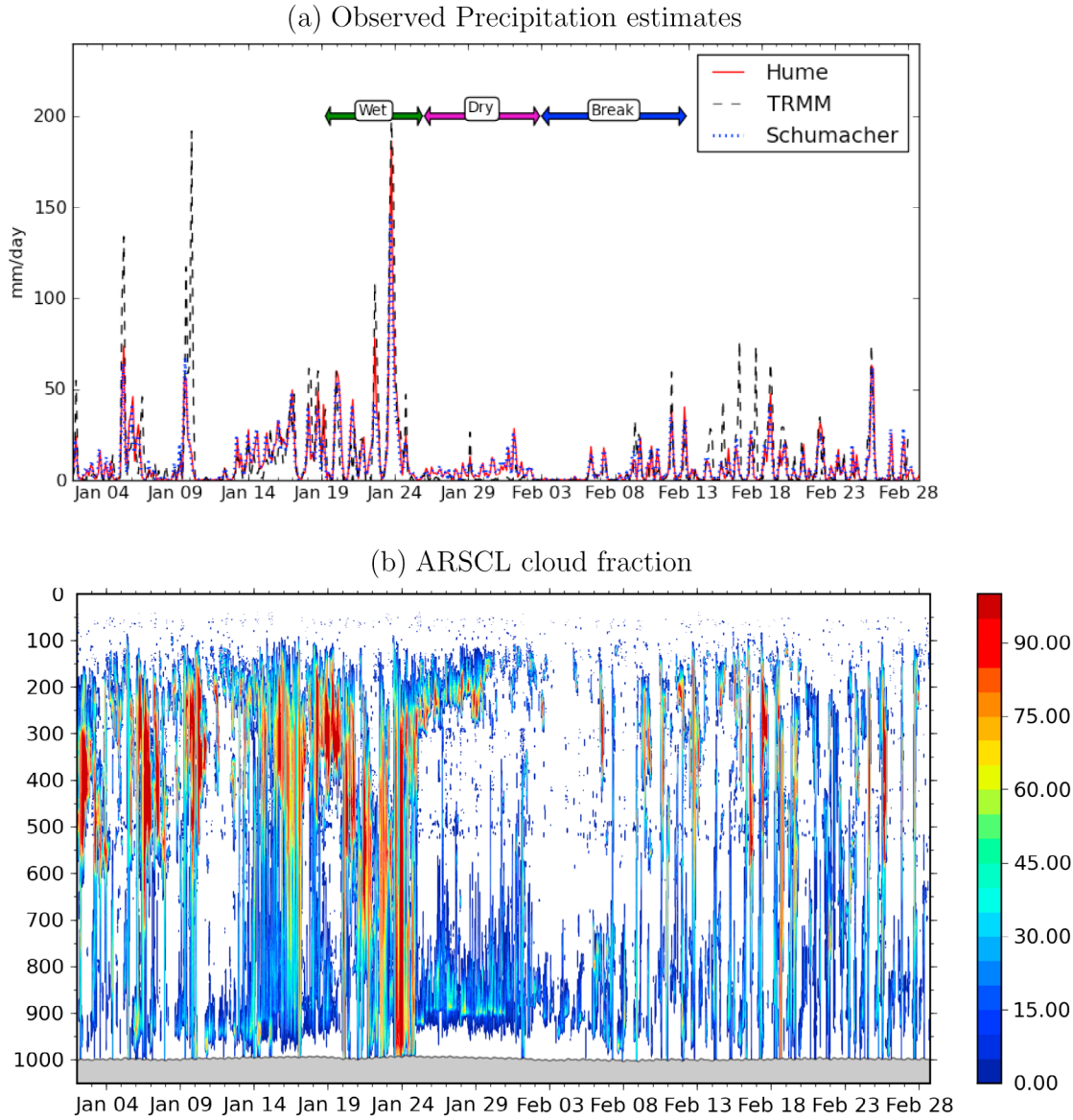


Figure 2. (a) Precipitation estimates from the C-POL radar (Hume and Schumacher) and TRMM averaged over TWP-ICE polygon (mm d^{-1}) and (b) Observed Cloud Frequency (ARSCL) at Darwin from the ARM cloud radar (percent). The C-POL radar observations are for 1 h intervals for the TWP-ICE polygon. TRMM estimates are a combination of satellite- and ground-based observations and are for 3 h intervals. The extents of the subperiods chosen for the TWP-ICE experiment are indicated on the precipitation plot.

cyclonic center inland resulted in torrential rain south of Darwin and very strong surface westerlies at Darwin. During this period, moderate amounts of rain fell from cumulus congestus clouds which are evident in the ARSCL observations. The Break period, 3–13 February, was characterized by a dissipation of the monsoon flow over the Australian/Indonesian region and the development of a heat trough dominating north Australia. Afternoon late day storms formed on the trough/sea breeze boundary. This gave rise to localized but fairly intense convective events along the coast.

[13] Also included in Figure 2 is the 3 h TRMM satellite rainfall estimate averaged over the same area as the radar. This is provided since later evaluations of model of rainfall beyond the TWP-ICE region will use the TRMM estimates.

The two estimates of rainfall based on the C-POL radar agree precisely on the timing of rain events and differ only slightly on the magnitude most of the time. Interestingly, TRMM fails to detect much of the precipitation during the Dry period. This indicates a limitation of the retrieval to discern rain from the middle level topped convection (con-

Table 1. Time Periods Used for Averaging Over TWP-ICE

Wet Monsoon (Active)	Dry Monsoon	Break
20 January to 25 January	26 January to 2 February	3 February to 13 February

gestus) present in this period. The TRMM also has several events which exceed the radar estimates by a large fraction.

2. Model Description and Initialization

[14] The general GCM used in this work is the atmosphere and land component of the Community Climate System Model version 4 (CCSM4) (P. R. Gent et al., The community climate system model version 4, submitted to *Journal of Climate*, 2010). The atmospheric model is designated as the Community Atmospheric Model 4 (CAM4). CAM4 is very similar in configuration to that described by Collins et al. [2006], with the exception of two changes made to the parameterization of deep convection. The convective parameterization changes are described by Neale et al. [2008] and will be briefly outlined below. All simulations use the finite volume dynamical core with the default 26 layers in the vertical. The parameterization of nonconvective cloud processes in CAM4 is that of Rasch and Kristjansson [1998] modified as in the work of Zhang et al. [2003]. The Rasch-Kristjansson scheme is a single moment bulk microphysical scheme with prognostic variables for the mass of stratiform ice and liquid. The stratiform condensation rate is based the grid scale relative humidity tendency following [Zhang et al., 2003].

[15] The deep convection parameterization in CAM is a bulk mass flux approach described in the work of Zhang and McFarlane [1995] (ZM). Closure in the ZM scheme is achieved by a rate limitation on the consumption of Convective Available Potential Energy (CAPE). The default implementation of ZM uses a traditional definition of CAPE which is calculated using an air parcel ascending pseudoadiabatically and not mixing with the environment. The technique used in the new closure, [Neale et al., 2008], allows mixing of the air parcel with environmental air depending on an assumed entrainment rate. This calculation makes the CAPE sensitive to the moisture profile above the boundary layer. The modification of the CAPE has a significant impact on the frequency and strength of convective events generated by the ZM scheme. The CAM sequentially calls two convective schemes. The first is the ZM scheme described above for penetrative convection and the second is the shallow convective parameterization of Hack [1994]. The ZM scheme computes the convective mixing of parcels coming from the lowest level. The Hack scheme is initiated when the parcel in the model layer immediately below is moist adiabatically unstable with respect to the current level. The adjustment to a stable state is accomplished over three model layers. As detailed in Richter and Rasch [2008], CAM4 uses a mass flux parameterization of momentum transport by deep convection based on Gregory et al. [1997].

[16] It is common practice to modify aspects of the model parameterizations when horizontal resolution is changed. As discussed by Hack et al. [2006], this process usually undertakes to obtain top of the model energy balance that is as close to observational estimates as possible across all model resolutions. A limited number of loosely constrained coefficients in the parameterized processes are varied to accomplish the desired result. In the standard CAM configuration a number of parameters are made functions of horizontal resolution (Table 2). To facilitate a clean comparison,

additional integrations were carried out with the 1°, 2° and 0.5° models having the identical settings to the 0.25° model including the time step. The 2° and 1° runs were also run with the recommended resolution dependent parameter settings seen in Table 2 and will be identified as “2°-T” and “1°-T”, respectively. Since the only difference in the 0.5° model was the time step, it was judged after some tests not to be worth the resources to run a “tuned” version for this resolution. It should be mentioned that the convective relaxation time used in the ZM scheme can be made a function of model resolution but in these experiments it is fixed at 1 h across all resolutions.

[17] The question of how best to compare the observational data at the TWP-ICE site with model output on various model grids is not straightforward. The model grids for the 2° and 0.25° models are shown in Figure 1. The TWP-ICE observations can be categorized roughly into a real means and point measurements. The region encompassed by the polygon in Figure 1 was intended to be on the order of a GCM grid cell. Its area is comparable to the coarsest model grid, 2°, used here. Even in this case the comparison is not exact since the model grid does not coincide with the polygon and thus some averaging needs to be done. For all the model grids, the comparison to the TWP-ICE a real mean was performed by taking a weighted mean of grid points surrounding Darwin, the weights being proportional to the area of overlap of the model grid box and the polygon.

[18] The model was initialized from operational analyses of the European Centre for Medium-Range Weather Forecasts (ECMWF) and National Center for Environmental Prediction (NCEP) Global Data Assimilation System (GDAS), which are available every 6 h on the native grid of the forecast model. The ECMWF data was on a 1° × 1° latitude-longitude grid with 91 levels on the model hybrid sigma coordinate. The GDAS was on a 0.465° × 0.465°, latitude-longitude grid with 64 levels in the model sigma coordinate. Thus variations at the finest scale of the 0.25° model are generated by CAM and are not directly propagating from the analysis used as the initial condition. The analysis data was interpolated in space to the CAM grid being careful to ensure consistency between the different representation of the surface topography between the CAM and the analyses [Boyle et al., 2008]. The sea surface temperatures used were weekly means based on the National Oceanic and Atmospheric Administration (NOAA) Optimum Interpolation analysis [Reynolds et al., 2002] and were linearly interpolated in time and space to the model discretization.

[19] The model was run as a NWP forecast model every 6 h. The initial conditions for each forecast for wind, temperature, surface pressure and moisture fields are from the analyses and all other atmospheric parameters and land variables are taken from the previous forecast without modification. The land component of all models was initialized for the first forecast from a climatological January specific for that model. The idea is to mimic the forecast/analysis cycle carried out at weather forecast centers. The extended forecasts were run for at least 3 days starting from 0000 UT. Model output from the second day of these forecasts, hours 24 to 48, are the basis for much of the evaluation undertaken in this paper. The day 2 forecasts are chosen as a compromise between being as close to the observed conditions as possible, but with enough simulation time to be comfortable that

Table 2. CAM Resolution-Dependent Parameters^a

Variable	$1.9^\circ \times 2.5^\circ$	$0.9^\circ \times 1.25^\circ$	$0.47^\circ \times 0.63^\circ$	$0.23^\circ \times 0.31^\circ$
Threshold for autoconversion of cold ice - RK (unitless)	9.5E6	18.0E6	45.0E6	45.0E6
Rainwater autoconversion coefficient - Hack (m^{-1})	1.0E-4	1.0E-4	5.0E-5	5.0E-5
Time step (s)	1800	1800	1800	900

^aThe default settings are shown. The 2° -T and 1° -T “tuned” models used the $1.9^\circ \times 2.5^\circ$ and $0.9^\circ \times 1.25^\circ$ settings, respectively. The other models, 2° , 1° , 0.5° , and 0.25° , used the setting shown for the $0.23^\circ \times 0.31^\circ$ line. The threshold for autoconversion of cold ice is used in the Rasch-Kristjansson cloud microphysics parameterization. The rainwater autoconversion coefficient is used in the Hack shallow convection parameterization. The time step is common throughout the model.

any initialization shock is small. The model rainfall spins up in the first 6 h of the forecast. When model time series are presented, they represent a concatenation of a series of day 2 forecasts, valid for the times indicated. The ECMWF analyses were used for all the simulations shown here but there did not appear to be any significant dependence on the analyses used.

3. Results

3.1. Rainfall

[20] Figure 3 presents CAM day 2 forecasts and the Hume observational estimates of 3 h rainfall over the TWP-ICE polygon for January and February 2006. It is seen that the models depict the time sequence of the observations fairly well, with the higher-resolution models capturing the variation more realistically. There is a definite, albeit not large difference between the tuned and untuned 2° and 1° forecasts with the tuned versions appearing to be better. The mean values of the observations for the two months are 9.4, 9.1 and 10.4 mm d^{-1} , for the Hume, Schumacher and TRMM data, respectively. The means of the models are larger with values of 10, 13, 11, 13.5, 14.8, and 16 mm d^{-1} for the 2° -T, 1° -T, 2° , 1° , 0.5° and 0.25° models, respectively.

[21] The largest observed rainfall occurs around 24 January 0000 UT. This event corresponds to a mesoscale convective system (MCS) passing over Darwin. The model curves all show a lag of 24 h in peak rainfall for this event, although this is less clear for 0.25° . This most likely results from the analysis data as the ECMWF forecast model precipitation also shows this lag. Similar lagged precipitation also resulted from use of GDAS analysis data. As the MCS circulation cannot be localized in space and time on the scales resolved by all the CAM versions, it should not be expected that the models capture the precise timing of convective events although we do expect the models to capture the essential aspects of the clouds and weather for the weather regimes identified above. The models’ Day 2 forecasts are slow to capture the rapid diminishment of observed rain from 24 January 0000 UT to 25 January 0000 UT. All models capture the light rain falling in the dry period between 24 January and 3 February. Note in Figure 2 that the TRMM data miss the rain over this period. Without the ground radar the models could have been deemed as too wet for these times. The models all show correct timing for the abrupt cessation of rain for 2 days after 4 February; apparently the large-scale forcing dictating this transition is well captured by all resolutions.

[22] Examining the effect of resolution, the higher-resolution models have greater peak values of precipitation.

The 0.25° time series is the only model which exhibits some peaks exceeding the observed. Furthermore, the 0.5° and 0.25° models better depict the variation of the rainfall with the on/off characteristic of the observations whereas the coarser resolution models have rainfall that persists at reduced magnitude between the peaks. This aspect is illustrated by Figure 4 which displays estimates of the autocorrelation of the hourly rainfall from the observations and models. There is a systematic increase in the model fidelity with resolution. The 0.25° model has a quite close correspondence to the observations for the first 10 h. Recall that the model rainfall is averaged over the observational polygon of Figure 1, so that differences in the character of the rainfall are not due to looking at a progressively smaller area. This persistence of rainfall may be important for the correct representation of tropical precipitation variability in models [Lin *et al.*, 2006].

[23] Figures 5a and 5b display histograms of hourly averaged precipitation for the 0.25° and 2° models and Hume C-POL radar observations over January and February 2006 for the TWP-ICE polygon. Only data from the two extreme resolution models are shown as the intermediate resolution models evince a fairly systematic progression between these two. The histogram for the 2° model has a tendency to cluster near 10 mm d^{-1} and is more symmetric than the observations. The finer resolution model diminishes the middle peak and spreads out to higher and lower values. While the 0.25° model exhibits better agreement with observations in the incidence of intense precipitation, there is an indication that this model has too much activity at the most intense rain rates of Figure 5. Consistent with Field and Shutts [2009], all models tend to underestimate the occurrence of rain in the lightest categories although this too is partially alleviated by increased resolution. Figures 5c and 5d compare histograms of daily mean rainfall from TRMM and the 0.25° and 2° models in the region of the Maritime continent (95°E to 150°E and 15°S to 15°N). All the data sets were coarse-grained to a $2^\circ \times 2^\circ$ common grid for the comparison. It can be seen that the characteristics of the comparison between models and observations seen at the TWP-ICE location carry over to the larger region. The 0.25° model again produces a more realistic distribution by both adding higher rain rates but also enhancing the very low rates. The negative skewness of the TRMM data over the Maritime continent seen in Figure 5 originates from observations over land, even though the land is only about 18 percent of the total Maritime continent area.

[24] Figure 6 displays the observed and modeled rainfall for a region enclosing the Maritime continent and Northern

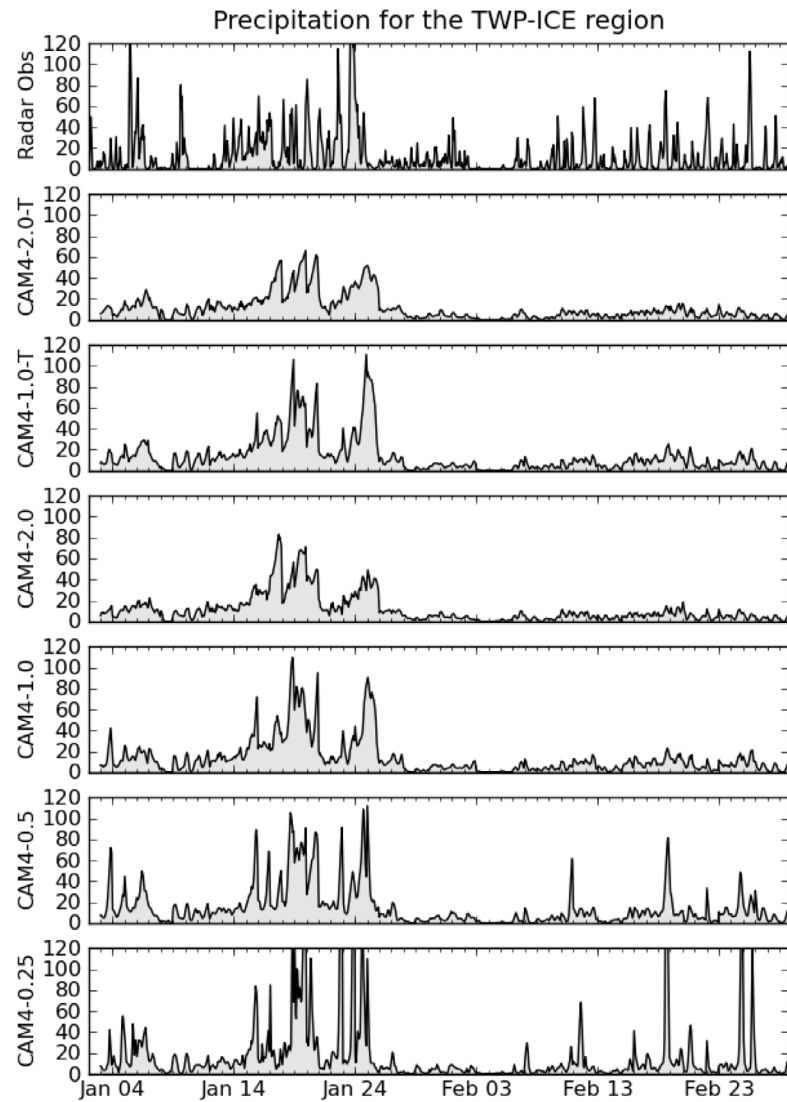


Figure 3. Radar-estimated (Hume) and modeled rainfall for January and February 2006. Data are for 1 h means within the TWP-ICE polygon. Units are mm d^{-1} .

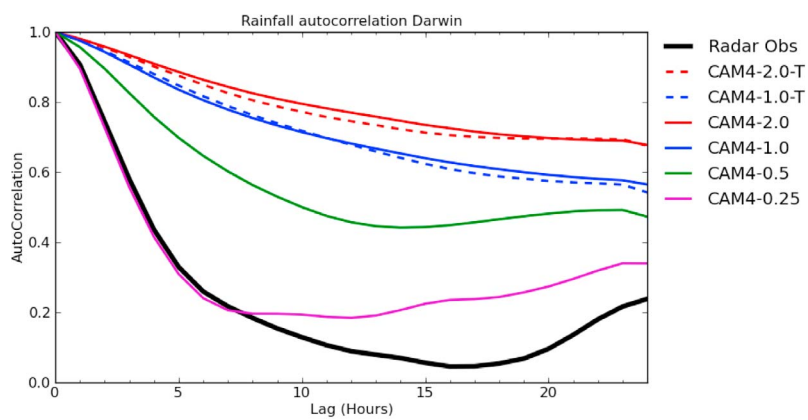


Figure 4. Autocorrelation estimates for Hume C-POL and modeled hourly rainfall for the TWP-ICE polygon.

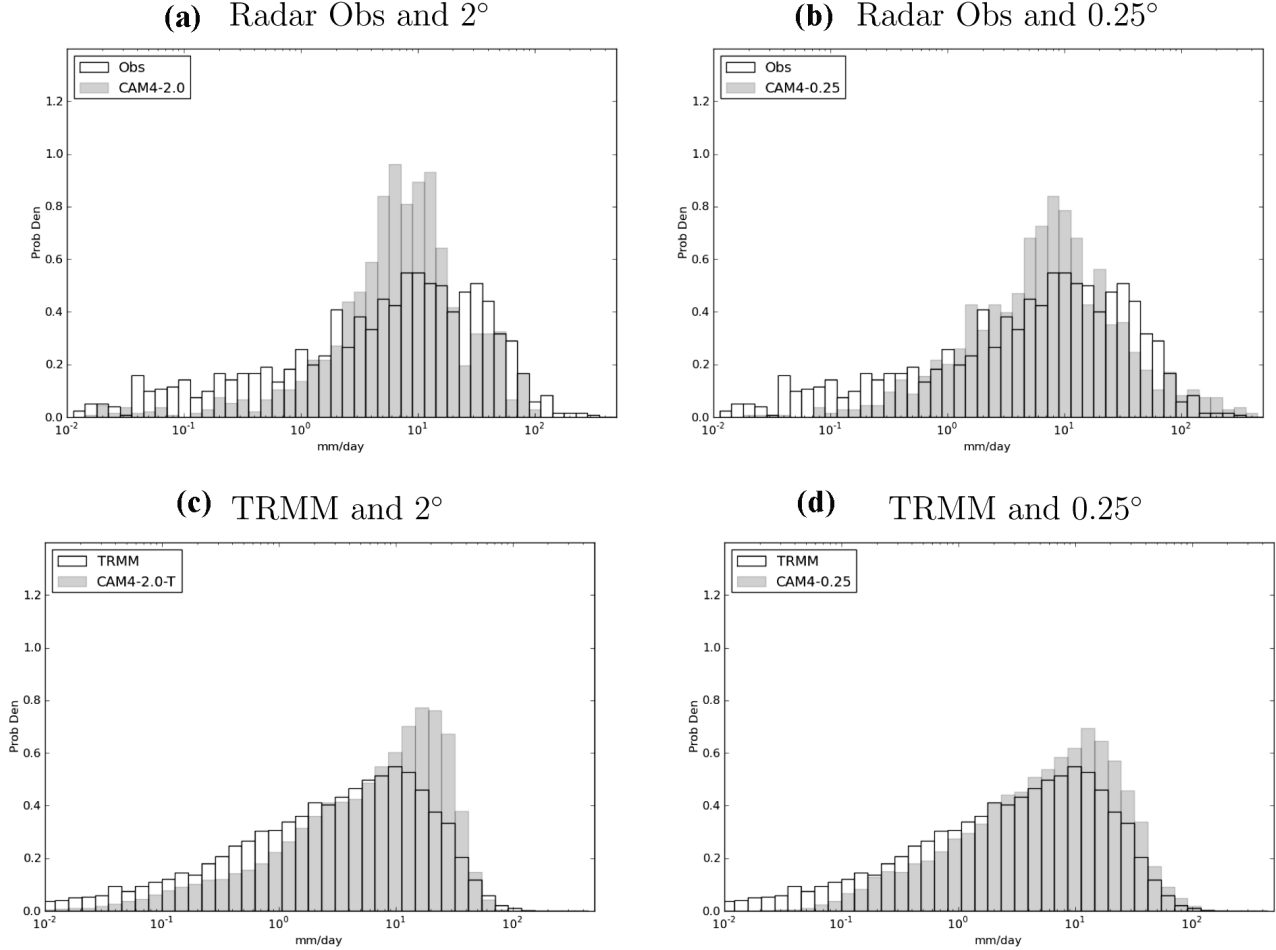


Figure 5. Histograms of observed and modeled rainfall for January and February 2006. (a, b) Hume C-POL radar hourly estimates and model data for the TWP-ICE polygon. (c, d) Daily means for the region 15°S–15°N, 105°E–155°E (Maritime Continent) from TRMM observations and model data. For Figures 5c and 5d, both the models and TRMM are coarse grained to a common 2° × 2° grid before computing the histogram. Units are mm d⁻¹.

Australia averaged over the 6 day TWP-ICE Wet period. Increasing resolution produces more sharply defined and more intense patterns. More importantly, these patterns are generally in agreement with the observations. An example of resolution improvement is the separate maxima for tropical cyclone Darryl at 120°E, 17°S by the 0.5° simulation. Zhao *et al.* [2009] also observed that tropical cyclones were resolved on a 0.5° grid in a GFDL model. The increasing resolutions tend to fill in detail upon the large-scale patterns set up by the 2° model, a characteristic seen in the work of Lau and Ploshay [2009] for the GFDL GCM. The 0.25° simulation appears to produce events which are perhaps too intense. During the Break period (not shown) the increased resolution improves the land-sea breeze diurnally forced circulations.

[25] Figure 7 shows the differences of the GPCP daily precipitation and models (day 2 forecasts) with respect to the TRMM observations averaged over January and February 2006. The pattern of the difference remains quite consistent across all the resolutions. The GPCP difference is provided to

give an indication of the observational uncertainty in rainfall. Only those regions with a model difference exceeding the difference in the observational estimates can be considered to be an error. A generalization is that the model overestimates the rainfall in the regions of observed heavy precipitation. This tendency is exacerbated by increasing resolution, particularly across the Pacific on either side of the Equator. This is a signature of the “split ITCZ” error which is endemic to many climate models and is not alleviated by resolution in this model. The lack of improvement with resolution is consistent with the results of Pope and Stratton [2002] who observed that increased resolution could accentuate errors apparent at lower resolutions, and Lau and Ploshay [2009] who found that the highest-resolution models also exhibited larger precipitation errors at the regional scale.

[26] The common aspect across the varied spatial regions considered is that the higher resolution provides better spatial and temporal characteristics at the expense of an increased overestimate of rainfall.

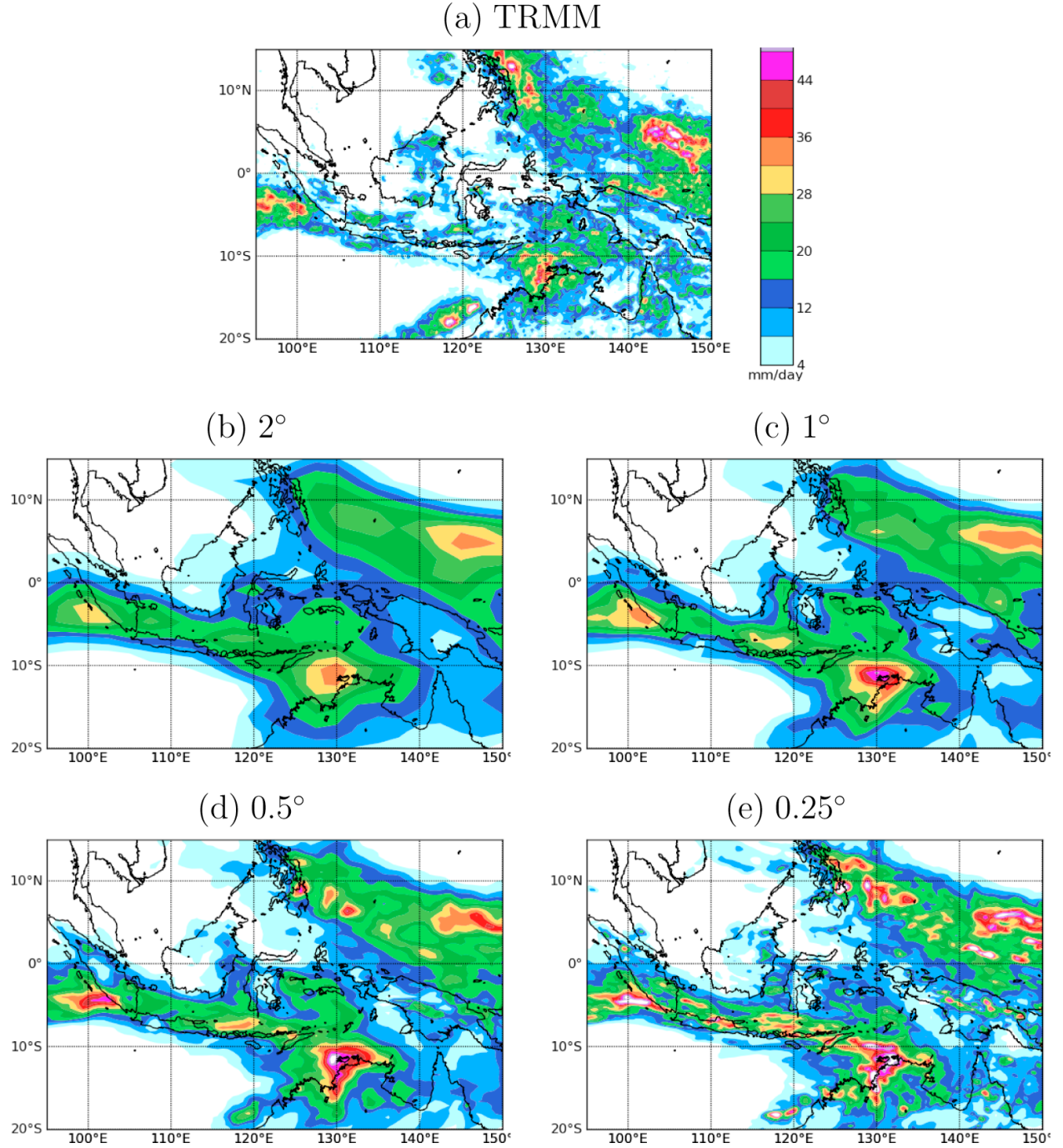


Figure 6. TRMM and modeled rainfall for the Maritime continent region averaged over the 6 day TWP-ICE Wet period. Units are mm d^{-1} .

3.1.1. Diabatic Heating: Q_1

[27] Closely related to the rainfall is the vertical profile of diabatic heating. Figure 8 displays vertical profiles of Q_1 [Yanai *et al.*, 1973] estimates from the variational analysis and the models averaged over the three periods for the TWP-ICE region. It is uncertain exactly how close a correspondence one should demand between the models and observations for Q_1 . This quantity is not directly observed but inferred from a number of sometimes poorly known forcings. Furthermore, the complex blend of land and water,

islands and mainland make for ambiguities in the site's representation in the lower resolution models. Finally, the experimental period is only 24 days divided into a few weather regimes. Nonetheless, the data available do present an opportunity to evaluate the models over a variety of tropical conditions in a region of importance to the global circulation. The VA ensemble does provide some measure of the effects of uncertainty in the rainfall observations on the heating estimates.

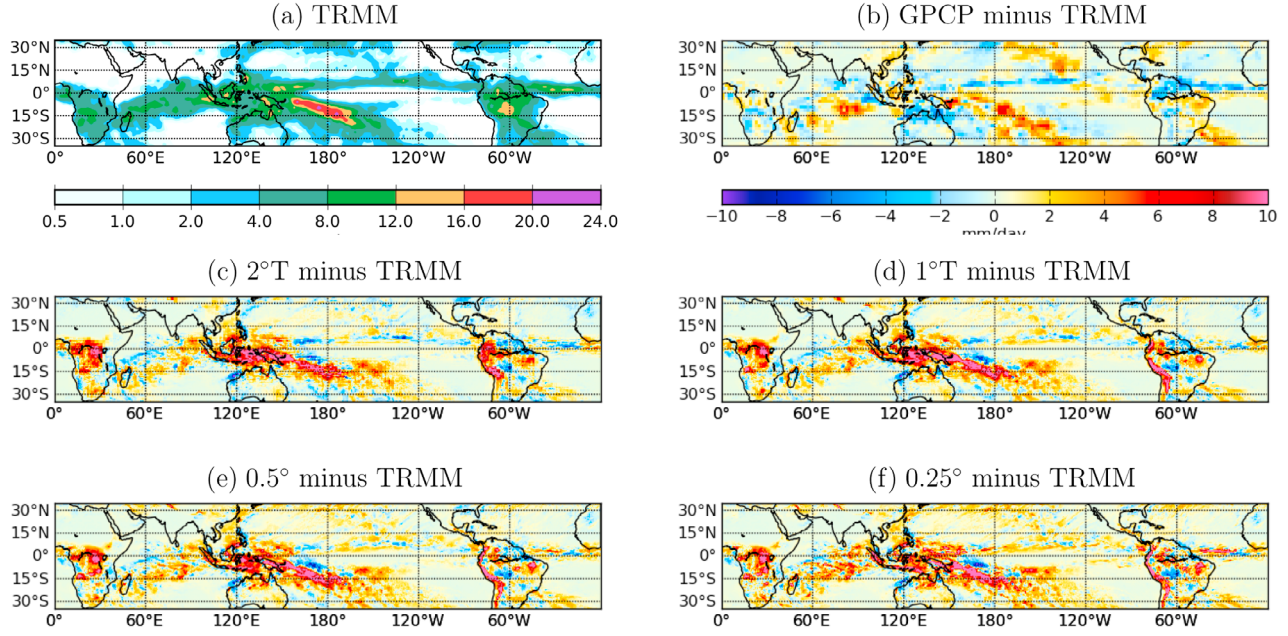


Figure 7. TRMM (a) observed rainfall and (b–f) differences GPCP and model differences from TRMM for January and February 2006. Units are mm d^{-1} . All difference plots (Figures 7b–7f) use the same color scale as in Figure 7b.

[28] For the Wet period (Figure 8a) the observational estimate indicates a broad peak centered about 400 hPa. The 2.0° model actually has the best fit to the observations. There is no evidence of a convergence to observations as the grid becomes finer, rather there is a systematic advance to higher values. All the models, save the 2.0° , exceed the 75th percentile of the VA ensemble below 800 hPa and above

300 hPa. The 0.25° model exceeds the 90th percentile at these levels. Consideration of the individual parameterizations suggests that the Hack and ZM convection schemes both contribute to the lower level overestimate. The partitioning of the heating is such that the ZM is the larger contributor in the 2.0° models and there is a transition such that the Hack is largest in the 0.25° model. The ratio is

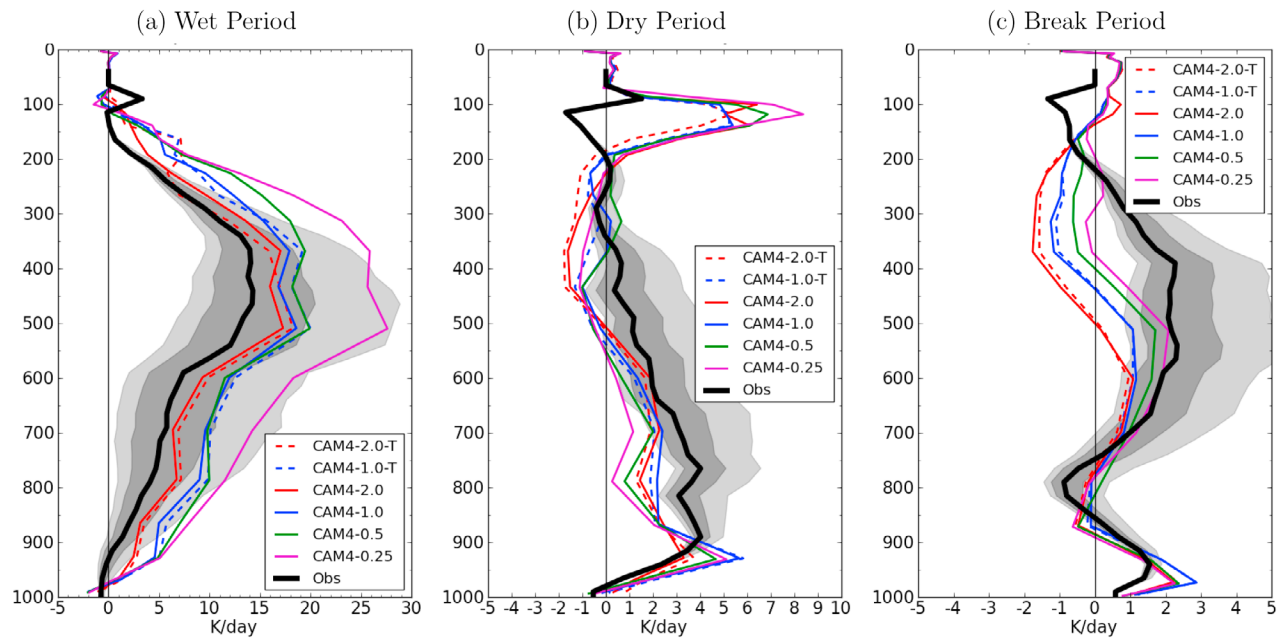


Figure 8. Variational analysis observations and modeled apparent heating for the TWP-ICE (a) wet, (b) dry, and (c) break periods. Note the change in scale between Figure 8a and Figures 8b and 8c. The dark shading encompasses the 25th and 75th percentiles of the analysis ensemble. The lighter shading encompasses the 10th and 90th percentile of the analysis ensemble. Units are $^{\circ}\text{K d}^{-1}$.

about a factor of two for the respective schemes at the extreme resolutions. At the upper levels the stable heating appears to make the critical contribution, and this increases with resolution.

[29] For the Dry period (Figure 8b) the heating is considerably reduced by about a factor of 4 compared to the Wet period. The observed Q_1 peak shifts to lower levels below 700 hPa. This is consistent with the cloud record of Figure 2, which indicates that the deep convection of the Wet period was replaced by congestus clouds. All models evince a reduction in heating from the Wet period and also shift the maximum heating to the lower troposphere. The model peak at 900 hPa is due to vertical temperature diffusion. Given the rather weak forcing, the correspondence of models and observations is fairly good and uniform across resolutions. All the models are now on the low side of the observations, for the most part below the 10th percentile of the VA ensemble between 900 and 300 hPa. Above 300 hPa, all the models have a very large overestimate of the cloud cover which leads to the Q_1 problems by way of radiation.

[30] The Break period (Figures 8c) has a modest heating peak at a vertical level somewhere between the peaks of the previous periods. The convective cells active during the Break period are isolated events along a land breeze front or over Tiwi Island. As seen in Figure 2, the rain during the Break is more intermittent and weaker than that of the Wet period. The models capture some of the shape of the Q_1 curve but fail to generate enough deep convection to drive the heating above the 500 hPa level. However, there are clear indications that the higher-resolution models are more successful in getting the heating to go deeper. Consideration of the components of the heating show that the ZM convection is the dominant source and the long wave cooling is the dominant sink for this period.

[31] Overall, the relative shifts in the level of maximum heating between the periods are discernable in the models without any obvious trends due to resolution. This suggests that the moist physics parameterizations of the model are responding reasonably well to the imposed large-scale state from the analyses.

3.1.2. Latent Heating

[32] Figure 9 displays the latent heating rates estimated from radar retrievals over the TWP-ICE polygon, [Schumacher *et al.*, 2007; Frederick and Schumacher, 2008], averaged over the indicated TWP-ICE periods. The Q_1 from the variational analysis is also plotted. The radar heating estimates are broken out into the contributions by convective and stratiform processes. Although Q_1 and latent heating are not expected to be identical since the Q_1 values include contributions to diabatic heating from radiation and subgrid scale turbulent fluxes, for these time scales the two should be fairly close above the boundary layer. Although not explicitly calculated, it is expected that the total latent heat profiles would exhibit a spread in estimates on the order of the VA ensemble Q_1 shown in Figure 8.

[33] During the Wet period, the contribution attributed to latent heating by the radar estimate peaks at a slightly lower level than Q_1 . The latent heating profiles indicate that the total profile shape is a result of the combination of the stratiform dipole structure and the more dominant convective contribution. This way of producing a top heavy heating

profile is described by *Lin et al.* [2004] and is deemed important to maintaining features such as the MJO by *Lin et al.* [2006]. The active phase of an MJO passed through Darwin during the Wet period of TWP-ICE. This combination of heating is also described to be typical for MCSs, [*Houze and Robert*, 2004; *Schumacher and Houze*, 2003]. During the Break and Dry periods the latent heating is virtually all convective. In both the Wet and Break periods the correspondence between the latent heating and Q_1 is good above the boundary layer where the latent heating is expected to dominate the diabatic heating. This tends to validate both data sets, since the vertical structure of the analyzed Q_1 depends on the rawinsonde profiles whereas the vertical structure of the radar latent heating depends on the profiles of radar reflectivity. Note that the Schumacher latent heating profiles are smooth due to the assumed shapes for the heating and because the C-POL has somewhat poorer vertical resolution than the variational analysis sonde data.

[34] Figures 10 and 11 contain model and the observational latent heating rates for the indicated TWP-ICE periods. There is a potential conceptual difference in the heating decomposition of Schumacher and that of the model. The model large-scale represents all resolved grid scale processes while the Schumacher data refers specifically to the stratiform structures associated with mesoscale convective systems. Nonetheless, for an appropriate parameterization suite and sufficient resolution, the model and Schumacher's concept may converge in regions with tropical deep convection.

[35] For the Wet period (Figure 10a) the observational estimate of the total latent heating indicates a broad peak centered about 450 hPa. The models have tended to extend the peak a bit high and values too large throughout the profile. The 2° models have the closest agreement with the observations. The large-scale heating dipole (Figure 10b) tends to be exaggerated in the models. The 0.25° model stands out with a large upper level heating and much reduced lower level evaporation. The other resolutions do not show large differences except 2° T at about 250 hPa. The transition of the 0.25° model is rather abrupt as there is little trend toward its profile as the resolution becomes finer. Examination of individual grid boxes (not shown) reveals that the 0.25° produces very high rain rates with a saturated or very nearly saturated lower troposphere. The model lower troposphere relative humidity and rainfall curves have a nature similar to the rain plots in Figure 3. The lower-resolution models have persistent rain and relative humidity with low values while the high resolutions have more episodic high rain rates and high relative humidity. The 0.25° takes this trend to the limit such that there are periods of 100% relative humidity which since cloud formation is tied to the relative humidity [Collins *et al.*, 2006] results in 100% cloud fraction. In the 0.25° model, the energy released due to conversion between vapor and condensate within stratiform cloud is slightly positive below 600 hPa while in all other models the contribution from this term is negative below 600 hPa. The cooling due to evaporation of large-scale rain is comparable between all the models and it is the condensational heating which drives the 0.25° model away from the other models below 600 hPa. The model convective component, Figure 10c, is larger below and above 500 hPa and this is not improved with higher resolution. The 2° model is the outlier, with a profile closer to the observed estimate.

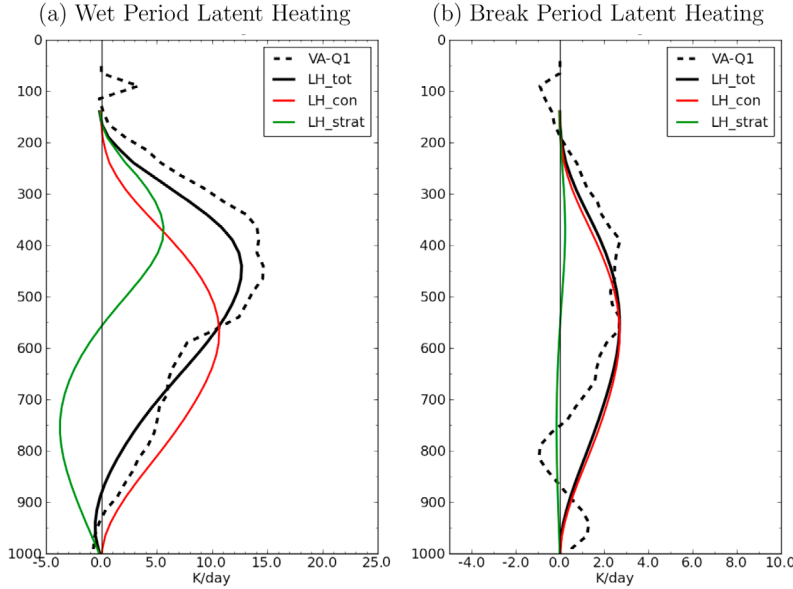


Figure 9. Radar estimated latent heating over the TWP-ICE region for the wet and break periods. Contributions to the heating are divided in stratiform (LH_{strat}), convective (LH_{con}), and total (LH_{tot}). Also shown is the Q_1 from the variational analysis (VA-Q1). Units are $^{\circ}\text{K d}^{-1}$.

[36] During the Dry and Break periods, large-scale latent heating plays a relatively minor role in the models and observations and thus only the total latent heating is shown (Figure 11). During the Dry period, the models underestimate the convective heating above 800 hPa and strongly overestimate it below. For the Break period the finer resolution models do slightly better in capturing the heating above 800 hPa than the lower resolution. This may be

because finer resolution allows for a better representation of land sea breeze circulations. For both the Dry and Break periods, the models capture the slight shift in the level of the maxima in the heating profiles.

3.1.3. Large-Scale and Convective Precipitation Ratio

[37] Table 3 lists the ratios of large-scale to total surface precipitation for the models and the observations for the Wet period over the TWP-ICE polygon and over the 20°N

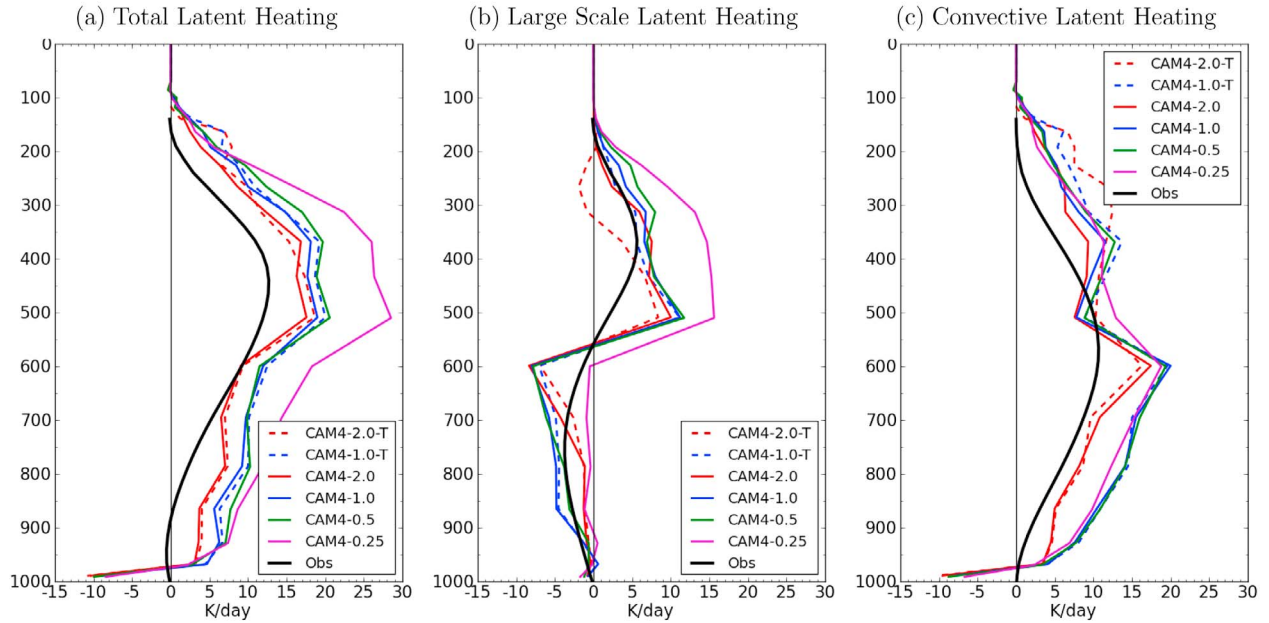


Figure 10. Radar estimated and modeled latent heating over the TWP-ICE polygon for the wet period. Contributions to (a) the total heating are divided into (b) large scale and (c) convective. Units are $^{\circ}\text{K d}^{-1}$.

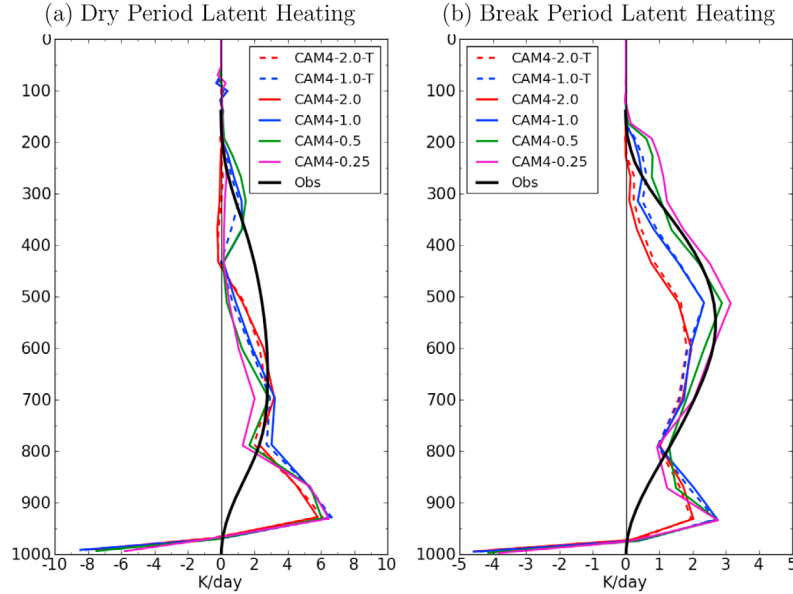


Figure 11. Radar estimated and modeled latent heating over the TWP-ICE polygon for the (a) dry and (b) break period. Only the total heating (convective + large scale) is presented. Units are $^{\circ}\text{K d}^{-1}$.

to 20°S band for January and February. Keep in mind that the definition of large scale for the observations does not exactly coincide with that of the models as previously discussed, although the agreement in the shape of the profiles in Figure 10b lends some credence to this comparison. As the resolution becomes finer, the ratio also increases to the point that the 0.25° model exceeds the observational estimate for the TWP-ICE wet period by a factor of two. For the tropical average a large increase is evident in going from the 0.5° to the 0.25° model. One must be cautious about conclusions from the data in Table 3 as the data are from a very small sample of time. Figure 12 displays the ratio of large-scale to total rainfall averaged over the latitude band from 20°N to 20°S around the globe for all the models averaged over January and February 2006. There is a systematic increase in the ratio with resolution. The 0.5° model has values on the order of the TRMM estimates and 0.25° model exceeds the observed. The observational values, Figure 3 of Schumacher and Houze [2003], analogous to Figure 12 are on the order of 40% with somewhat less longitudinal variation.

[38] It is interesting to note that the increase in the fraction of precipitation that is large scale can be achieved through parameterization instead of resolution changes. For example, Lin *et al.* [2008] tested a number of convective parameterizations and moisture triggers for atmospheric GCMs. Their model experiments generated a spread of values comparable to Figure 12, although their results had less longitudinal variation than were found here. Lin *et al.* [2008] also indicate that greater contributions to the large-scale condensation can produce better simulations of convectively coupled equatorial waves. It is also of interest to determine how increased resolution leads to greater large-scale precipitation fraction. The standard expectation is that the finer resolution grids make it easier to achieve the threshold relative humidity for stratiform cloud formation and thus

could be expected to produce more stratiform rain, as seen in the simulations of Duffy *et al.* [2003] using an earlier version of the CAM. The present experiments indicate that the increase in surface stratiform precipitation is achieved through an increase in large-scale condensation aloft and the fact that this increased rainfall is not accompanied by a concomitant increase in evaporation in the nearly saturated lower troposphere of the 0.25° model.

3.2. Apparent Drying: Q_2

[39] Figure 13 displays the apparent drying (Q_2) [Yanai *et al.*, 1973] for the observations and models for the periods of TWP-ICE. During the Wet period, the 0.25° model is an outlier with the drying exceeding or near the 90th percentile of the VA ensemble. All the models are probably removing water in excess of observed below 600 hPa. Below

Table 3. Ratio of the Large-Scale (Stratiform for Observations) to Total Rainfall for Day 2 Forecasts at TWP-ICE for the Wet Period and for the Tropical Region 20°N to 20°S Over January and February 2006 and for the AMIP Integrations for the Tropical Region 20°N to 20°S Over January and February 2006^a

Model	TWP-ICE Wet Period	Tropics January and February	AMIP Tropics January and February
$1.9^{\circ} \times 2.5^{\circ}$	25	22	20
Tuned			
$1.9^{\circ} \times 2.5^{\circ}$	38	26	28
$0.9^{\circ} \times 1.25^{\circ}$	31	26	24
Tuned			
$0.9^{\circ} \times 1.25^{\circ}$	38	29	29
$0.47^{\circ} \times 0.63^{\circ}$	41	36	31
$0.23^{\circ} \times 0.31^{\circ}$	62	47	46
Schumacher Observation	32	≈ 40	≈ 40

^aUnits are in percent (%).

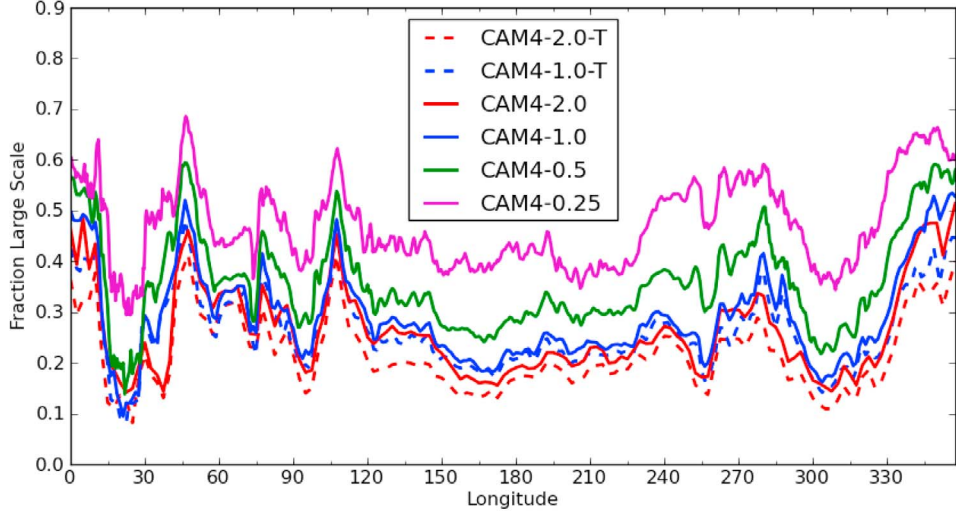


Figure 12. Model fraction of large-scale precipitation compared to total precipitation averaged from 20°S to 20°N for January and February 2006.

800 hPa all model show excessive drying beyond the 90th percentile of the ensemble. Aloft, the models do capture an upper level peak, albeit with a peak at too high a level and too high values. The agreement in the other two periods is poor, and the finer grid only slightly addresses the problems. The removal by the deep convection appears to be relatively uniform across the resolutions. During the dry period, the models establish midtropospheric evaporation ($Q_2 < 0$) similar to the observations. During the break period the relative shape of the Q_2 profile in the models and observations is anticorrelated.

3.3. Diurnal Variation Over the Maritime Continent

[40] The rainfall over the Maritime continent plays a key role in the circulation of the Tropics and the globe [Neale and Slingo, 2003]. The resolution experiments of Neale and Slingo [2003] indicate that the diurnal cycle over the islands and the complex circulation patterns generated by land-sea contrasts are crucial for the energy and hydrological cycles of the Maritime Continent and for determining mean climate. Using a regional model of 25 km grid resolution [Qian, 2008] performed 30 year integrations with

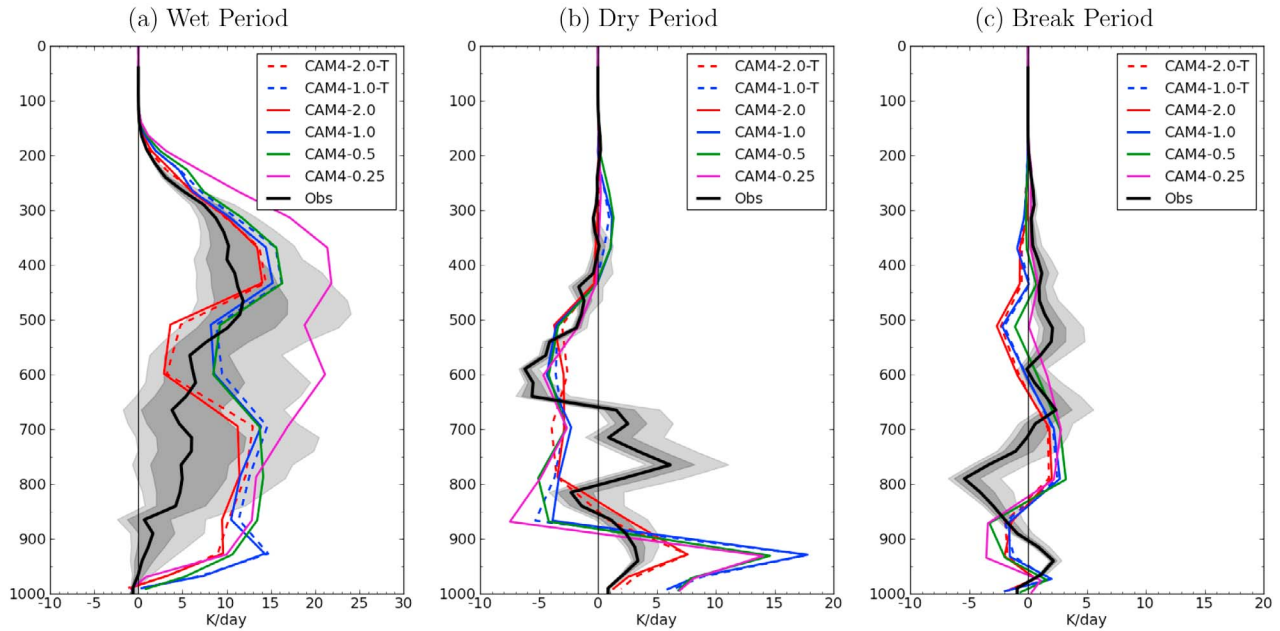


Figure 13. Variational analysis and modeled apparent drying for the TWP-ICE wet period. The dark shading encompasses the 25th and 75th percentiles of the analysis ensemble. The lighter shading encompasses the 10th and 90th percentile of the analysis ensemble. Units are $^{\circ}\text{K d}^{-1}$.

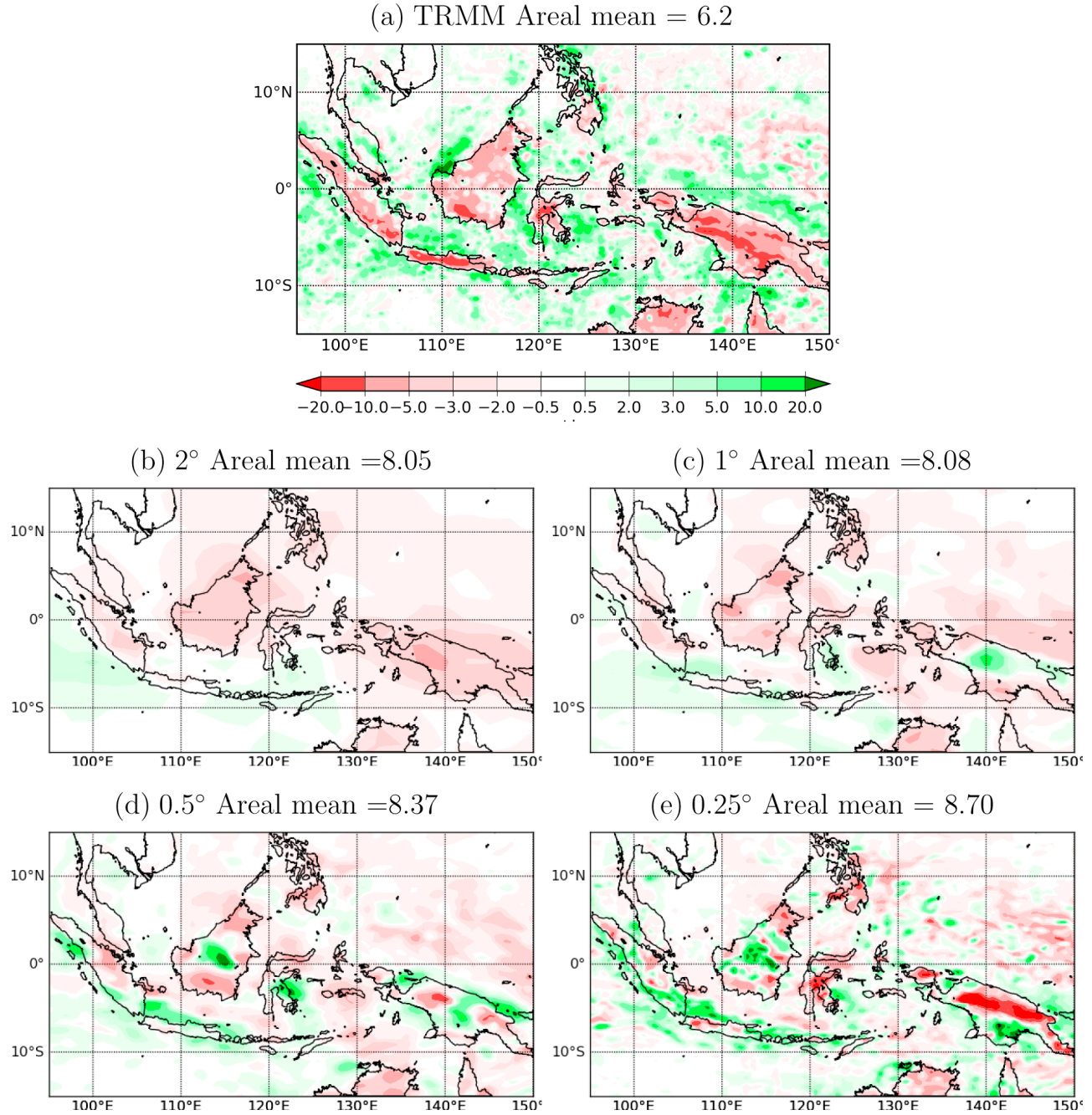


Figure 14. TRMM and modeled precipitation at 0000 UT averaged over January and February 2006 with the daily mean removed. Captions include the mean rainfall over the depicted region. Units are mm d^{-1} .

prescribed monthly mean SSTs to investigate the nature of the precipitation over the Maritime Continent. He found that the precipitation is concentrated on the islands by diurnally forced sea-breeze convergence, and the under representation of the island topography will result in an underestimate of the region's precipitation. Arakawa and Kitoh [2005] found that circulations and rainfall over the Maritime Continent were well simulated by JMA climate model run with approximately 20 km horizontal grid spacing.

[41] Figure 14 shows the January and February mean 0000 UT rainfall from TRMM and the models with the daily

mean having been subtracted. 0000 UT is 8AM local time at 120°E and is about the time of the peak of the observed rain over the ocean. This time was chosen to illustrate a pattern of relative extrema in the land-sea contrasts of the diurnal cycle. Kikuchi and Wang [2008] states that the TRMM data used here (3B42) is adequate to describe most aspects of the diurnal cycle and they provide an analysis of the diurnal cycle over the Maritime continent which corresponds well with Figure 14. The amplitude variation of the peak diurnal variations is over a factor of three in going from the 2° to the 0.25° model. The dipoles which form in the observations

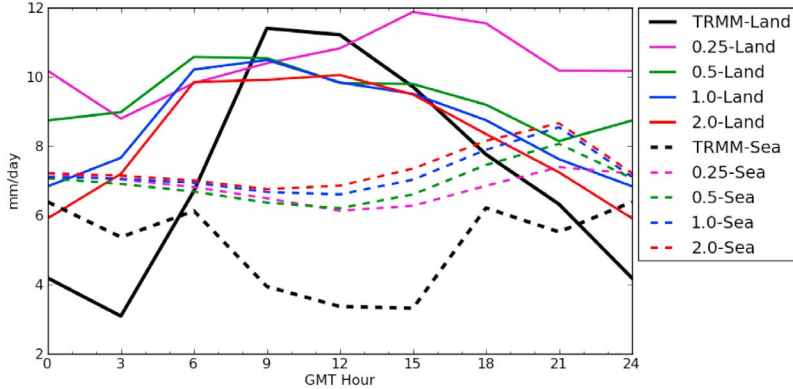


Figure 15. TRMM and model rainfall diurnal cycle averaged for January and February 2006. Data are averaged over land (solid lines) and sea (dashed lines) for the region 15°S – 15°N and 95°E – 130°E . Land (sea) is determined by a grid box having land (sea) fraction greater than 0.7. Here 0000 UT corresponds to about 0800 local time in this region.

about the islands of Java, Sumatra and New Guinea have been shown to be due to gravity currents generated by the uneven heating of mountainous land and ocean and not by advection of the island rain to offshore, [Arakawa and Kitoh, 2005]. The model does a good job at high resolution of reducing precipitation over land except in central Borneo where there is an anomalous precipitation maximum. While the increased resolution clearly improves the simulation of the diurnal cycle over this region, this does not translate into correcting the model bias in regional mean rainfall. As seen in Figure 7, the region has an over estimate of rain with respect to TRMM across all the model resolutions which increases slightly with finer resolution. In all cases, the models overestimate the rain, and if anything this gets worse with increasing resolution. Figure 15 shows the diurnal cycle over land and ocean within the region 95°E to 130°E and 15°S to 15°N from TRMM and the untuned models. The models underestimate the amplitude of the diurnal cycle over both land and ocean by nearly a factor of two when compared to TRMM and this is not improved by increased horizontal resolution. The problem appears to be too much rain by the models during the morning over land leading to a peak in precipitation that is 3 h too early and insufficient diminishment of the model rain over the ocean during the early evening. Neale and Slingo [2003] expressed an optimism that an improved representation of the diurnal cycle resulting from higher horizontal resolution would improve the model bias. This does not appear to be true for the CAM.

[42] Figure 16 shows the surface divergence and winds at 0000 UT for the models and the GDAS analysis (which we show because it has the finest resolution of the analyses available to us). The surface wind of the GDAS analysis is for the most part forced by the forecast model used in the assimilation. The point here is that a climate model is capable of generating detailed circulations comparable to a state of the art forecast system; how realistic these circulations are is another matter. Higher-resolution models capture details of the complex flow between the islands. The diurnal alteration of the surface convergence and divergence becomes very well defined as resolution increases in reasonable correspondence to the precipitation. The 0.25° sur-

face divergence compares well with the high-resolution GCM results of Arakawa and Kitoh [2005] and the regional model simulations of Qian [2008] as well as that computed from the GDAS analyses. It appears that resolution of at least 0.5° is required to capture the land-sea breeze circulations about the maritime continent using the CAM.

4. Discussion

[43] The question implicit in any study of climate model resolution is that of assessing what is to be gained by using higher resolution and whether this gain is worth the additional resources. The unsatisfactory answer is that it depends on the context for which the model results are to be used. For the Maritime continent region (Figure 14), the areal average rainfall is essentially constant across all the resolutions with an overestimate with respect to TRMM of about 30%. If the main concern is simulating the gross heating in this region, which is important for the global circulation, then the gain represented by an order of magnitude increase in computation expense is marginal. However, if the detailed distribution of rainfall is important then the increased resolution is essential. As found by Gent *et al.* [2009], the better resolved topography drives the model to produce more realistic rainfall patterns in the vicinity of topography. As seen in Figures 6 and 14, the patterns of rainfall will be quite different in the finer resolution models even if the area averaged bias remains. As pointed out by Gent *et al.* [2009], these pattern changes can have a large effect on the modeled river flows and other aspects of the land hydrology. The ability of the higher-resolution models to simulate the intermittency of rainfall (Figure 4) is also a positive aspect for hydrologic models.

[44] It is perhaps telling that the best agreement in the diabatic heating is with the 2° models (Figure 8). This might be due to the fact that most development effort has been carried out at this resolution. Nonetheless, a factor of eight increases in resolution appears to only drive the estimates to excessive values. Pope and Stratton [2002] indicate that parameterizations probably need to be revised or replaced as resolution increases due to nonlinear effects that can generate errors unique to each resolution. We note

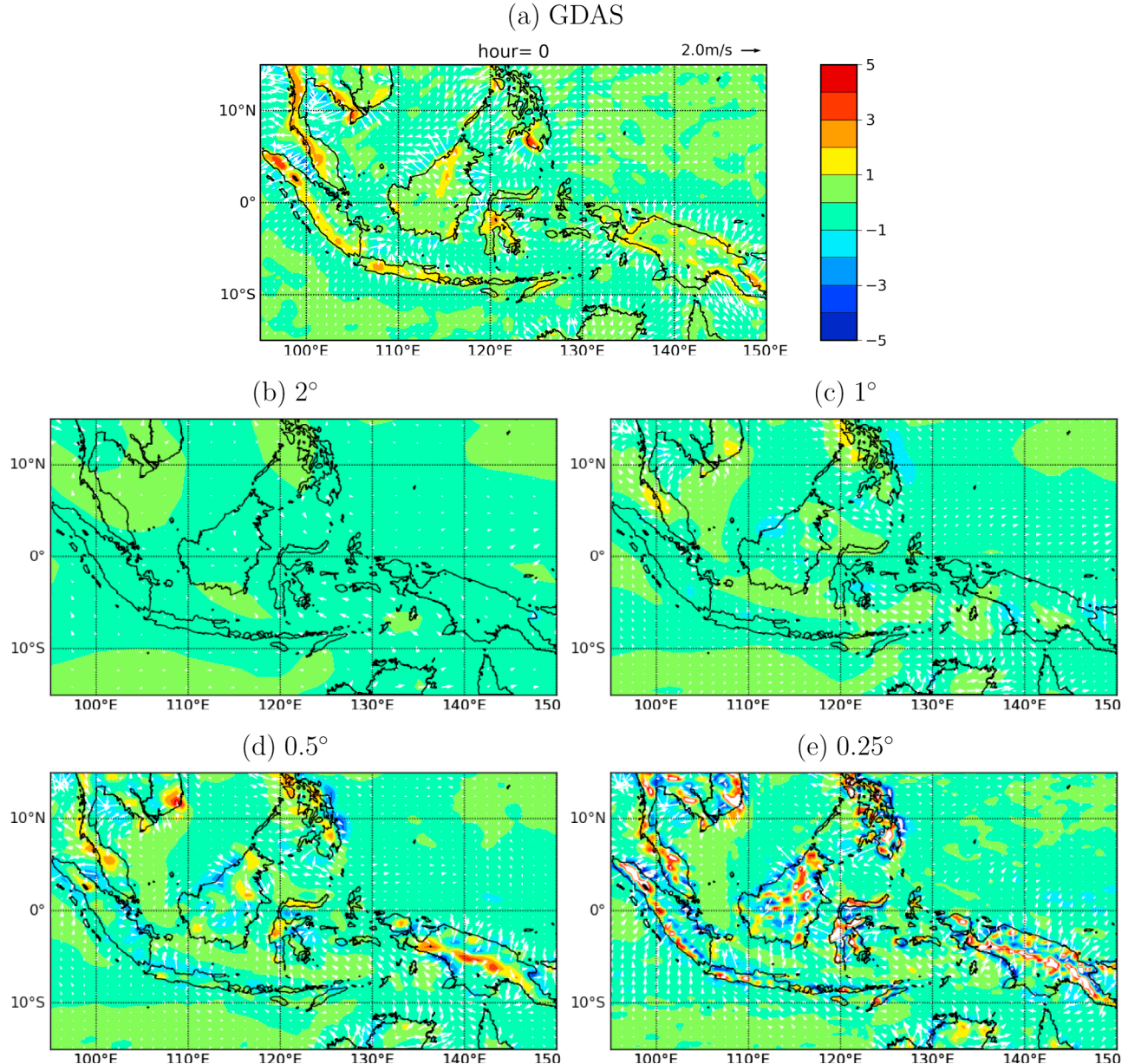


Figure 16. GDAS and modeled surface divergence (colors) and wind (vectors) at 0000 UT averaged over January and February 2006 with the daily mean removed. The scale for the wind is on the top right of each plot. Divergence units are s^{-1} , and wind units are $m s^{-1}$. For clarity, the vectors are thinned for the higher resolutions.

that the 0.25° model has had only a small amount of development and thus continued exploration of parameter settings in climate and forecast integrations could lead to substantial improvements.

[45] Despite little change in the area-averaged rainfall, we note the following improvements with higher horizontal resolution. First, CAM produced diurnal circulations that appear to be as least as realistic as leading NWP forecast centers and regional models for the Maritime Continent. Second, CAM also shows an increase in the ratio of stratiform to convective rainfall with increased resolution (perhaps too large), which should have a positive impact on convectively coupled waves [Lin *et al.*, 2008]. Finally, the

temporal variability and intensity of rainfall is more realistic at higher resolution as seen in the time series of Figure 3.

[46] In going to finer resolutions the relative burdens placed on the suite of model parameterizations can change. The current integrations make it clear that the 0.25° model will have a great deal more grid resolved latent heating, some of which may be excessive. Thus, the robustness of the parameterization of this heating becomes critical at higher resolution. Lin *et al.* [2008] demonstrated that the ratio of large-scale to total precipitation can be strongly affected by the deep convection parameterization. An experiment with a preliminary version of the Morrison-Gettelman [Gettelman *et al.*, 2008] two moment cloud

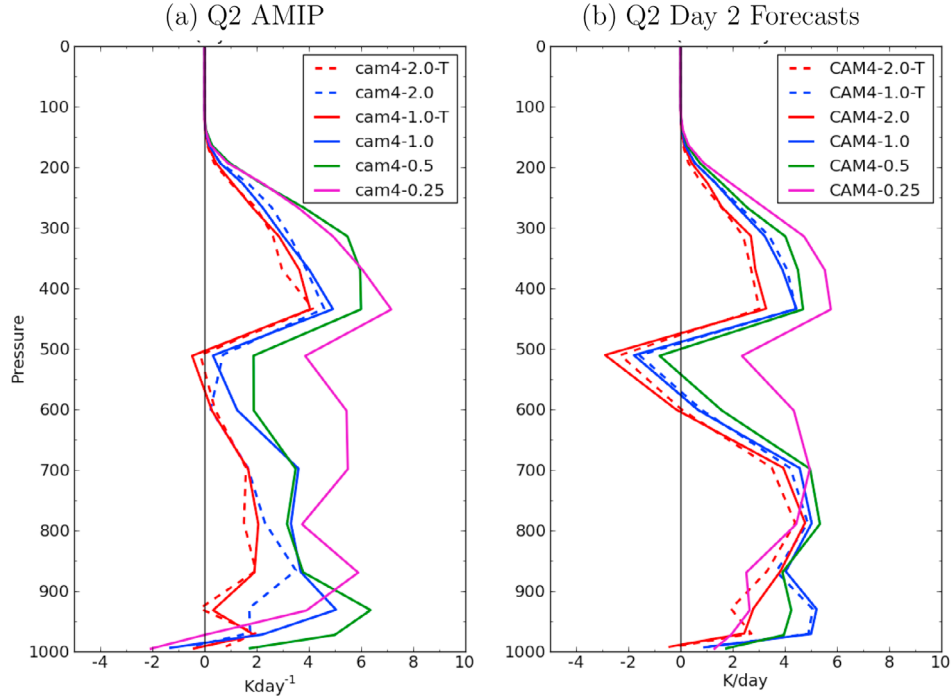


Figure 17. Apparent drying at the TWP-ICE polygon averaged over January and February 2006 for (a) AMIP simulations and (b) day 2 forecasts. Units are $^{\circ}\text{K d}^{-1}$.

microphysics replacing the Rasch-Kristjansson was run using CAM 3.5 which is similar to CAM 4. The use of this alternate parameterization reduced to ratio of large-scale to convective rainfall for all resolutions with a factor of 2

reduction for the 0.25° model for Tropics as compared to Table 3.

[47] In order to understand how these results from forecast simulations translate to climate simulations AMIP type

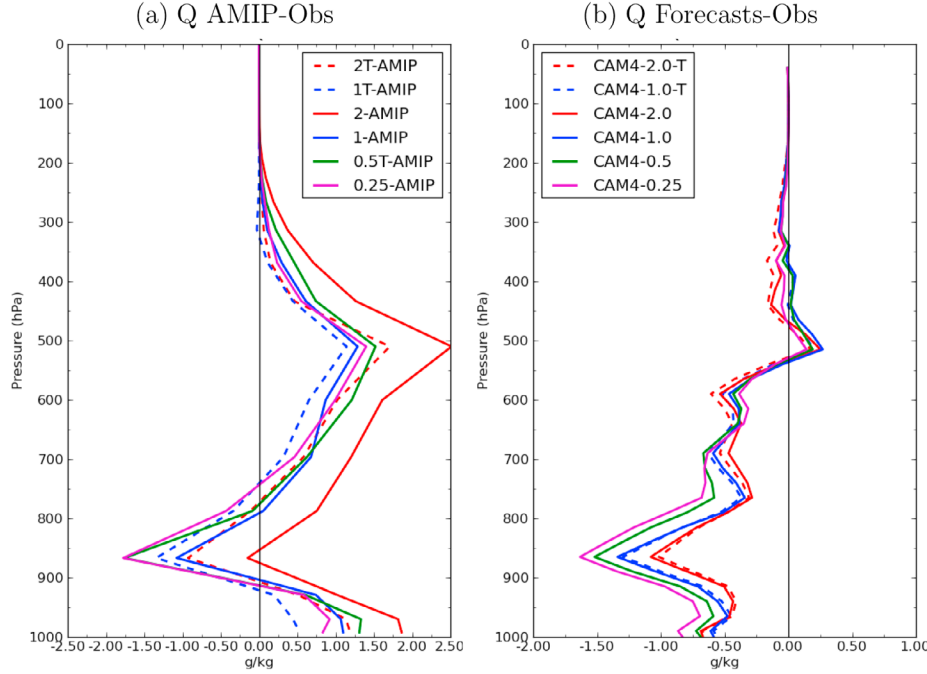


Figure 18. Modeled minus observed specific humidity differences at the TWP-ICE polygon. (a) CAM4 AMIP simulations for January and February 2006. (b) Day 2 CAM4 forecasts for the entire TWP-ICE experiment. Units are g kg^{-1} .

simulations were performed for all resolutions over January and February 2006 using the same observed SSTs as in the forecasts. The AMIP simulations were initiated in September 2005 and run for 6 months. Overall, the January and February day 2 forecasts and AMIP averages were similar for the variables used in this paper. For example, the increase with resolution in the ratio of large-scale to total precipitation (Table 3) is very similar in the AMIP integrations as well as the model forecasts. As another example, Figure 17 shows the Q_2 for the AMIP runs and the day 2 forecasts at the TWP-ICE polygon averaged over January and February. It is apparent that the dependence of Q_2 on horizontal resolution is similar in the forecasts and free running simulations. In the AMIP simulations, the differences generated by the resolution are convolved with the chaotic differences as the models move through a succession of distinct states. In the forecasts the models are forced through a specific series of states which in a sense isolates the differences due to resolution alone. What is gained by the forecasts is the ability to make use of detailed observations. Figure 18 compares the differences between observations of specific humidity and the AMIP simulation and the Day 2 forecasts at the TWP-ICE site for January and February 2006. It can be seen that the tendencies with model resolution seen in the forecasts carry over to the climate type of simulation, at least in the lower troposphere where the models become drier as the resolution increases. There is even a correspondence in the shape of the difference curves between the forecasts and AMIP runs in Figure 18. Although more work is needed, it does provide some indication that the information on the model performance gleaned from the TWP-ICE forecasts has implications for model's climatology. It should also be noted that the sensitivity to the model tuning becomes somewhat more evident for the longer-term simulations. The tuned and untuned models show a large difference in 2° models Figure 18.

5. Conclusions

[48] The CAM 4.0 was run as a forecast model starting from ECMWF and NCEP global analyses. The model was run for the period of January and February 2006 during which the TWP-ICE experiment provided detailed heating profiles and precipitation data for the 1.5° region about Darwin, Australia. Day 2 forecast results were analyzed and allow the model parameterizations to be evaluated outside of model biases which will develop in longer-term climate integrations. The model was run with nominal horizontal resolutions of 2° , 1° , 0.5° , and 0.25° and 26 vertical levels. Analysis of the integrations showed that the CAM is capable of producing credible simulations across a broad range of resolutions. Tuning the model generally improves the simulations, but the model response to tuning is complex and the choice of the final parameter values will probably require substantial effort. Circulation features such as tropical cyclones were somewhat more realistically represented in the 0.5° and 0.25° simulations compared to the coarser models.

[49] Compared to the heating profiles computed for the TWP-ICE experiment, the model produced credible simulations when consideration is taken for the uncertainty endemic to these observations. Particularly encouraging is the generally good simulation of heating profiles in very

different weather regimes, which indicates that the model's parameterizations respond properly to the change in large-scale state imposed by the analyses. Comparisons to observed diabatic drying rates were less favorable. There was no obvious progression toward the observations in the heating rates across resolutions except in that the depth of land-sea breeze convection during the break period is greater and closer to observed with higher resolution.

[50] The global biases of precipitation with respect to the TRMM observations had very similar patterns across resolutions, and the agreement did not improve with increasing resolution. There was a systematic shift toward observational estimates of the ratio of convective to large-scale rainfall as resolution was increased. Additionally, the model simulated reasonable vertical profiles of large-scale and convective heating and their relative amounts. The spatial pattern of the diurnal variation of rainfall and surface wind over the Maritime continent demonstrated a dramatic improvement at finer resolution. For this aspect of the simulations the 0.25° model compared favorably to published regional integrations and operational NWP forecasts.

[51] This resolution exercise with the CAM4 shares many of the aspects of the resolutions studies cited in the Introduction. It would be of interest to see if the parameterization improvements of the CAM5 will lead to a better overall performance at high horizontal resolution.

[52] **Acknowledgments.** We are grateful to the European Center for Medium-Range Weather Forecasts and National Center for Environmental Prediction for making their operational analyses available. Courtney Schumacher generously supplied latent heating estimates for the TWP-ICE. Timothy Hume provided high-resolution precipitation data for the months of January and February 2006. We thank Peter Caldwell and Shaocheng Xie for providing comments on the manuscript. The variational analyses and other observational data were obtained from the ARM program sponsored by the U.S. Department of Energy, Office of Science, Office of Biological and Environmental Research, Environmental Sciences Division. Work at LLNL was performed under the auspices of the U.S. Department of Energy by Lawrence Livermore National Laboratory under contract DE-AC52-07NA27344. The efforts of the authors were funded by the Regional and Global Climate Modeling and Atmospheric System Research programs of the U.S. Department of Energy as part of the Cloud-Associated Parameterizations Testbed (CAPT).

References

- Ackerman, T. P., and G. Stokes (2003), The atmospheric radiation measurement program, *Phys. Today*, **56**, 38–45.
- Adler, R. F., et al. (2003), The version-2 Global Precipitation Climatology Project (GPCP) monthly precipitation analysis (1979–present), *J. Hydrometeorol.*, **4**(6), 1147–1167.
- Arakawa, O., and A. Kitoh (2005), Rainfall diurnal variation over the Indonesian maritime continent simulated by 20 km-mesh GCM, *SOLA*, **1**, 109–112.
- Boyle, J., S. Klein, G. Zhang, S. Xie, and X. Wei (2008), Climate model forecast experiments for TOGA COARE, *Mon. Weather Rev.*, **136**, 808–832.
- Clothiaux, E. E., T. P. Ackerman, G. G. Mace, K. P. Moran, R. T. Marchand, M. A. Miller, and B. E. Martner (2000), Objective determination of cloud heights and radar reflectivities using a combination of active remote sensors at the ARM CART sites, *J. Appl. Meteorol.*, **39**(5), 645–665.
- Collins, W. D., et al. (2006), The formulation and atmospheric simulation of the Community Atmosphere Model version 3 (CAM3), *J. Clim.*, **19**(11), 2144–2161.
- Duffy, P. B., B. Govindasamy, J. P. Iorio, J. Milovich, K. R. Sperber, K. E. Taylor, M. F. Wehner, and S. L. Thompson (2003), High-resolution simulations of global climate: Part 1. Present climate, *Clim. Dyn.*, **21**, 371–390.
- Field, P. R., and G. J. Shutts (2009), Properties of normalised rain-rate distributions in the tropical Pacific, *Q. J. R. Meteorol. Soc.*, **135**, 175–186.

- Frederick, K., and C. Schumacher (2008), Anvil characteristics as seen by C-POL during the Tropical Warm Pool International Cloud Experiment (TWP-ICE), *Mon. Weather Rev.*, **136**(1), 206–222.
- Gent, P. R., S. G. Yeager, R. B. Neale, S. Levis, and D. A. Bailey (2009), Improvements in a half degree atmosphere/land version of the CCSM, *Clim. Dyn.*, **34**(6), 819–833, doi:10.1007/s00382-009-0614-8.
- Gettelman, A., H. Morrison, and S. J. Ghosh (2008), A new two-moment bulk stratiform cloud microphysics scheme in the Community Atmosphere Model, Version 3 (CAM3): Part II. Single-column and global results, *J. Clim.*, **21**(15), 3660–3679.
- Gregory, D. R., R. Kershaw, and P. M. Inness (1997), Parameterization of momentum transport by convection: II. Tests in single-column and general circulation models, *Q. J. R. Meteorol. Soc.*, **123**, 1153–1183.
- Hack, J. J. (1994), Parameterization of moist convection in the National Center for Atmospheric Research Community Climate Model (CCM2), *J. Geophys. Res.*, **99**(D3), 5551–5568, doi:10.1029/93JD03478.
- Hack, J., J. M. Caron, G. Danabasoglu, K. W. Oleson, C. Bitz, and J. Truesdale (2006), CCSM-CAM3 climate simulation sensitivity to changes in horizontal resolution, *J. Clim.*, **19**(11), 2267–2289.
- Houze, J., and A. Robert (2004), Mesoscale convective systems, *Rev. Geophys.*, **42**, RG4003, doi:10.1029/2004RG000150.
- Huffman, G. J., R. F. Adler, D. T. Bolvin, G. Gu, E. J. Nelkin, K. P. Bowman, Y. Hong, E. F. Stocker, and D. B. Wolff (2007), The TRMM multisatellite precipitation analysis (TMPA): Quasi-global, multiyear, combined-sensor precipitation estimates at fine scales, *J. Hydrometeorol.*, **8**(1), 38–55.
- Kikuchi, K., and B. Wang (2008), Diurnal precipitation regimes in the global tropics, *J. Clim.*, **21**(11), 2680–2696.
- Lau, N.-C., and J. J. Ploshay (2009), Simulation of synoptic- and subsynoptic-scale phenomena associated with the East Asian summer monsoon using a high-resolution GCM, *Mon. Weather Rev.*, **137**(1), 137–160.
- Lin, J., B. Mapes, M. Zhang, and M. Newman (2004), Stratiform precipitation, vertical heating profiles, and the Madden Julian oscillation, *J. Atmos. Sci.*, **61**(3), 296–309.
- Lin, J.-L., et al. (2006), Tropical intraseasonal variability in 14 IPCC AR4 climate models: Part I. Convective signals, *J. Clim.*, **19**(12), 2665–2690.
- Lin, J.-L., M.-I. Lee, D. Kim, I.-S. Kang, and D. M. W. Frierson (2008), The impacts of convective parameterization and moisture triggering on AGCM-simulated convectively coupled equatorial waves, *J. Clim.*, **21**(5), 883–909.
- May, P. T., J. H. Mather, G. Vaughan, C. Jakob, G. M. McFarquhar, K. N. Bower, and G. G. Mace (2008), The tropical warm pool international cloud experiment, *Bull. Am. Meteorol. Soc.*, **89**(5), 629–645.
- Neale, R., and J. Slingo (2003), The maritime continent and its role in the global climate: A GCM study, *J. Clim.*, **16**(5), 834–848.
- Neale, R. B., J. H. Richter, and M. Jochum (2008), The impact of convection on ENSO: From a delayed oscillator to a series of events, *J. Clim.*, **21**(22), 5904–5924.
- Pope, V. D., and R. A. Stratton (2002), The processes governing horizontal resolution sensitivity in a climate model, *Clim. Dyn.*, **19**, 211–236.
- Qian, J.-H. (2008), Why precipitation is mostly concentrated over islands in the maritime continent, *J. Atmos. Sci.*, **65**(4), 1428–1441.
- Rasch, P. J., and J. E. Kristjansson (1998), A comparison of the CCM3 model climate using diagnosed and predicted condensate parameterizations, *J. Clim.*, **11**, 1587–1614.
- Reynolds, R., N. Rayner, T. Smith, D. Stokes, and W. Wang (2002), An improved in situ and satellite SST analysis for climate, *J. Clim.*, **15**, 1609–1625.
- Richter, J. H., and P. J. Rasch (2008), Effects of convective momentum transport on the atmospheric circulation in the community atmosphere model, version 3, *J. Clim.*, **21**(7), 1487–1499.
- Schumacher, C., and R. A. Houze (2003), Stratiform rain in the tropics as seen by the TRMM precipitation radar, *J. Clim.*, **16**(11), 1739–1756.
- Schumacher, C., M. H. Zhang, and P. E. Ciesielski (2007), Heating structures of the TRMM field campaigns, *J. Atmos. Sci.*, **64**(7), 2593–2610.
- Shaffrey, L. C., et al. (2009), U.K. HiGEM: The new U.K. high-resolution global environment model-model description and basic evaluation, *J. Clim.*, **22**(8), 1861–1896.
- Xie, S., T. Hume, C. Jakob, S. A. Klein, R. B. McCoy, and M. Zhang (2010a), Observed large-scale structures and diabatic heating and drying profiles during TWP-ICE, *J. Clim.*, **23**(1), 57–79.
- Xie, S., et al. (2010b), CLOUDS AND MORE: ARM climate modeling best estimate data, *Bull. Am. Meteorol. Soc.*, **91**(1), 13–20.
- Yanai, S., M. Esbensen, and J.-H. Chu (1973), Determination of bulk properties of tropical cloud clusters from large-scale heat and moisture budgets, *J. Atmos. Sci.*, **30**, 611–627.
- Zhang, G. J., and N. A. McFarlane (1995), Sensitivity of climate simulations to the parameterization of cumulus convection in the Canadian Climate Centre general circulation model, *Atmos. Ocean*, **33**, 407–446.
- Zhang, M. H., and J. L. Lin (1997), Constrained variational analysis of sounding data based on column-integrated budgets of mass, heat, moisture, and momentum: Approach and application to ARM measurements, *J. Atmos. Sci.*, **54**(11), 1503–1524.
- Zhang, M. H., J. L. Lin, R. T. Cederwall, J. Yio, and S. C. Xie (2001), Objective analysis of ARM IOP data: Methods and sensitivity, *Mon. Weather Rev.*, **120**(1), 295–311.
- Zhang, M., W. Lin, C. S. Bretherton, J. J. Hack, and P. J. Rasch (2003), A modified formulation of fractional stratiform condensation rate in the NCAR Community Atmospheric Model (CAM2), *J. Geophys. Res.*, **108**(D1), 4035, doi:10.1029/2002JD002523.
- Zhao, M., I. M. Held, S.-J. Lin, and G. A. Vecchi (2009), Simulations of global hurricane climatology, interannual variability, and response to global warming using a 50 km resolution gcm, *J. Clim.*, **22**(24), 6653–6678.

J. Boyle and S. A. Klein, Lawrence Livermore National Laboratory, L-103, LLNL/PCMDI, 7000 East Ave, Livermore, CA 94550-9234, USA. (boyle5@llnl.gov)